

1

2 The effect of sample drying temperature on marine 3 particulate organic carbon composition

4 Sarah Z. Rosengard^{1,2*}, Phoebe J. Lam³, Ann P. McNichol^{4,5}, Carl G. Johnson², Valier V.
5 Galy²

- 6 1. Massachusetts Institute of Technology Department of Earth, Atmospheric and
7 Planetary Sciences, Cambridge, MA, U.S.A.
- 8 2. Woods Hole Oceanographic Institution Department of Marine Chemistry and
9 Geochemistry, Woods Hole, MA, U.S.A.
- 10 3. University of California-Santa Cruz Department of Ocean Sciences, Santa Cruz,
11 CA, U.S.A.
- 12 4. Woods Hole Oceanographic Institution Department of Marine Geology and
13 Geophysics, Woods Hole, MA, U.S.A.
- 14 5. National Ocean Sciences Accelerator Mass Spectrometry Facility, Woods Hole,
15 MA, U.S.A.

16
17 Corresponding author contact: (tel) 646-361-1195; srosengard@eoas.ubc.ca

18 * current affiliation: University of British Columbia Departments of Geography and
19 Earth, Ocean and Atmospheric Sciences, Vancouver, BC, Canada

20
21 Keywords: particulate organic carbon composition, sample drying treatment, ramped
22 oxidation

23
24

25 **Abstract**

26

27 Compositional changes in marine particulate organic carbon (POC) throughout
28 the water column trace important processes that underlie the biological pump's
29 efficiency. While labor-intensive, particle sampling efforts offer potential to expand the
30 empirical POC archive at different stages in the water column, provided that organic
31 composition is sufficiently preserved between sampling and analysis. The standard
32 procedure for preserving organic matter composition in marine samples is to immediately
33 store particles at -80°C to -20°C until they can be freeze-dried for analysis. This report
34 investigates the effect of warmer drying and storage temperatures on POC composition,
35 which applies to the majority of POC samples collected in the field without intention for
36 organic analysis. Particle samples collected off Woods Hole, MA were immediately dried
37 at 56°C, at room temperature, or stored at -80°C until being freeze-dried. Results show
38 that oven- and air-drying did not shift the bulk composition (i.e., carbon and nitrogen
39 content and stable isotope composition) of POC in the samples relative to freeze-drying.
40 Similarly, warmer drying temperatures did not affect POC thermal stability, as inferred
41 by ramped pyrolysis/oxidation (RPO), a growing technique that uses a continuous
42 temperature ramp to differentiate components of organic carbon by their decomposition
43 temperature. Oven- and air-drying did depress lipid abundances relative to freeze-drying,
44 the extent of which depended on compound size and structure. The data suggest that field
45 samples dried at room temperatures and 56°C are appropriate for assessing bulk POC
46 composition and thermal stability, but physical mechanisms such as molecular
47 volatilization bias their lipid composition.

48 **1 Introduction**

49

50 Marine particulate organic carbon (POC) is the primary vector for the biological
51 pump, which transfers ~0.2 Gt carbon/year - approximately 0.1 % marine primary
52 productivity - to the seafloor (Burdige 2007). These particles harbor thousands of distinct
53 organic biomolecules generated predominantly by primary producers and heterotrophs
54 (Repeta 2014). Changes in this biomolecular matrix in the water column reflect important
55 processes that govern the transport and recycling of marine POC (Burd et al. 2016).
56 Techniques for describing changes in this matrix range from measuring bulk
57 characteristics that are an integration of all biomolecules (e.g., the stable isotope
58 composition of total POC, reported as $\delta^{13}\text{C}$) to quantifying smaller abundances of specific
59 biomolecules (e.g., the abundance of lipid biomarkers and their $\delta^{13}\text{C}$ values) (Wakeham
60 and Volkman 1991; Trull and Armand 2001; Cavagna et al. 2013).

61 To accurately interpret the composition of POC in the water column, its organic
62 matrix must be preserved between collection and analysis. Prior studies have
63 demonstrated a link between wet sample storage temperature and organic matter
64 preservation. For example, storage at room temperature can promote microbial
65 degradation in the sample matrix, significantly altering the distribution of lipid
66 abundances after one month (Grimalt et al. 1988). But, even longer term storage at
67 temperatures below freezing can alter the lipid composition of organic matter by
68 rupturing cell membranes and concentrating enzymes in solution, increasing the
69 extraction efficiency of free fatty acids and preferentially breaking down polar lipids
70 (Wakeham and Volkman 1991; Ohman 1996). Current recommendations are that marine

71 samples intended for organic analysis are frozen immediately after collection and stored
72 at -80°C to -20°C and freeze-dried prior to analysis, which minimizes alteration of
73 organic matter composition by heterotrophic remineralization after sampling (Wakeham
74 and Volkman 1991).

75 Still, the majority of particulate matter collected at sea is not intended for organic
76 analysis. Samples for bulk elemental analysis are often dried in a heated oven, and
77 samples for inorganic analysis are sometimes air-dried, and then stored at room
78 temperature before analysis (e.g., Buesseler et al. 2005; Bishop and Wood 2008; Bishop
79 et al. 2012; Lam et al. 2015; Rosengard et al. 2015), rather than being freeze-dried. The
80 tremendous labor, financial cost and scientific potential of sampling marine particles
81 warrants an investigation into how much POC integrity is sacrificed when different
82 sample drying methods do not meet optimal standards of organic geochemical analysis
83 (Wakeham and Volkman 1991). This paper compares the effects of freeze-drying
84 samples, air-drying samples at room temperature, and oven-drying samples at elevated
85 temperatures on three aspects of organic composition: bulk organic matter composition
86 (C/N ratio, $\delta^{13}\text{C}$ and total organic carbon content), biomolecular composition (specific
87 lipid abundances), and thermal stability.

88 In this report, the latter metric for composition, thermal stability, refers to the
89 distribution of temperatures over which a POC sample decomposes to CO_2 during
90 ramped pyrolysis/oxidation (RPO), a novel but increasingly utilized technique for
91 characterizing the composition of organic matter in the environment. By pyrolyzing or
92 oxidizing POC throughout a controlled temperature ramp from ~100°C to 800°C, and
93 monitoring the release of CO_2 throughout the ramp, this technique differentiates distinct

94 pools of bulk organic carbon by their thermal stability, reflecting the activation energy of
95 decomposition/oxidation of specific POC pools in the sample (Cramer 2004). RPO has
96 been applied over a range of organic matter samples from complex depositional
97 environments, from suspended riverine POC to ocean sediments (Rosenheim et al. 2008;
98 Rosenheim and Galy 2012; Rosenheim et al. 2013; Subt et al. 2016). Thus, RPO of
99 marine POC offers a unique opportunity to relate POC composition to its biological
100 reactivity in the environment, which impacts the strength of the biological pump
101 (Francois et al. 2002; Burd et al. 2016).

102 We hypothesized that air-drying and oven-drying a sample would negligibly
103 influence the bulk composition and thermal stability of POC (e.g., Kaehler and
104 Pakhomov 2001). The energy imposed by high-flow air-drying and oven-drying relative
105 to freeze-drying is too small to shift the bonding energies (Wagner et al. 1994) and
106 therefore the activation energies of thermal decomposition in the biomolecular matrix
107 (Cramer 2004). Moreover, these approaches dry particle samples within 24 hours, which
108 likely minimizes microbial degradation of POC in the sample. By contrast, we expected
109 air-drying and oven-drying to shift the absolute and relative abundances of specific
110 biomolecules in POC, which are typically present in trace quantities. Indeed, Wang et al.
111 (2017) observed that lipid distributions in soils shifted in response to heating at
112 temperatures as low as 60°C. The results of these comparisons have several implications
113 towards the opportunistic use of marine particle samples for organic analysis, even when
114 not processed according to ideal organic geochemical standards.

115

116 2 Materials and procedures

117

118 Different drying treatments were compared using samples of marine POC
119 collected off the dock of the Woods Hole Oceanographic Institution (WHOI), at
120 41.524°N, 70.672°W, in June 2014.

121

122 2.1 Sample collection

123

124 To collect marine particles, a battery operated *in situ* pump (McLane WTS-LV)
125 was deployed ~10 meters below surface and pumped seawater through two identical flow
126 paths (Lam et al. 2015). Each flow path directed seawater through a 51 μm pore-size
127 polyester pre-filter screen followed by a pair of pre-combusted 1 μm pore-size quartz
128 fiber filters (Whatman™ quartz membrane grade A, or QMA), both mounted onto “mini-
129 MULVFS” filter holders (Bishop et al. 2012). The active collection area of these filters
130 was 125 cm^2 . The pre-filter retained $>51 \mu\text{m}$ size-fraction particles, while the QMA
131 collected 1-51 μm size-fraction particles, most of which settled on the first QMA filter of
132 the flow path. After ~45 minutes, or 40-100 L seawater filtered, the filters clogged and
133 the pump stopped.

134 The pump was deployed twice, collecting two pre-filters and two pairs of sample
135 QMA filters (POC1 and POC2) over both flow paths in the first deployment, and one pre-
136 filter and one pair of QMA filters (POC3) from one flow path in the second deployment
137 (Table 1). During each deployment, a deployment blank sample was also collected by
138 submerging a complete filter set - a 51 μm pre-filter and a pair of QMA filters -

139 sandwiched between 1 μm mesh filters to exclude particles, in a perforated plastic
140 Tupperware box, which was externally attached to the McLane pump frame. The second
141 pump deployment immediately followed the first. Depth control was poor, so the two
142 deployments likely occurred at slightly different depths.

143 Of all filters deployed, only the QMA filters, which collected $<51 \mu\text{m}$ particles,
144 were analyzed. Of the three pairs of particle filters collected, only the topmost QMA filter
145 relative to the pump's flow path was analyzed, as this filter likely retained most $<51 \mu\text{m}$
146 particles (Fig. 1a, c). For each pair of the two deployment blank filters, we considered
147 differences between the two QMA filters to be negligible (Fig. 1b). Each sample and
148 deployment blank filter was divided into thirds prior to drying, such that each drying
149 treatment could be applied in triplicate. As Section 3 argues, this dividing scheme helped
150 account for environmental heterogeneity associated with particle sampling in POC-rich
151 waters during analysis of thermal and lipid composition of the samples (Sections 2.3-2.4).
152 One third was immediately frozen at $\sim -10^\circ\text{C}$, transferred to -80°C two weeks later, and
153 finally freeze-dried overnight before analysis (Fig. 1, Table 1). Another third was placed
154 in an oven for drying at 56°C for 17-19 hours. Finally, one third was dried under a clean
155 laminar flow hood at high air flow and room temperature for 17-19 hours. All oven-dried
156 and air-dried filters were stored in Whirl-Pak bags or combusted glassware at room
157 temperature before analysis. All analyses were done within one year of sample collection.

158 Prior to analysis, images of dried QMA filters were developed at various
159 magnifications for a freeze-dried portion of deployment blank and sample filters using a
160 scanning electron microscope (SEM) (Fig. 1b, c). No coccoliths or other calcium
161 carbonate shells were observed in the sample filter. Thus, we assumed that the particulate

162 inorganic carbon content (PIC) in the particle samples was negligible, and would not
163 interfere with any of the POC analyses described in the following sections. The stable
164 isotope data reported in the “Assessment” section will address this assumption.

165

166 **2.2 Bulk composition analysis**

167

168 The bulk composition (particulate organic carbon concentration ([POC]),
169 particulate nitrogen concentration ([PN]), $\delta^{13}\text{C}$ and $\delta^{15}\text{N}$) of the dried QMA filters was
170 analyzed using a *Fisons Instruments Carlo / Erba 1108* elemental analyzer interfaced via
171 a *Finnigan MAT Conflo II* to a *Thermo Finnigan Delta-Plus* stable isotope ratio mass
172 spectrometer. These analyses were intended to guide our choice of filter sub-sample size
173 for ramped pyrolysis/oxidation (RPO) analysis, while maximizing the amount of sample
174 left for RPO and lipid analysis (Section 2.3). Thus, for each drying treatment, only ~0.9%
175 of the active area of a whole QMA filter (125 cm²) from a different filter replicate was
176 analyzed in bulk: the freeze-dried sub-sample of particle filter POC2, the air-dried sub-
177 sample of filter POC3, and the oven-dried sample of filter POC1 (Table 1). One
178 deployment blank sub-sample (~0.9% QMA active area) from a freeze-dried filter portion
179 was analyzed, as well.

180

181 **2.3 Ramped oxidation analyses**

182

183 The ramped pyrolysis/oxidation (RPO) system at the National Ocean Sciences
184 Accelerator Mass Spectrometry (NOSAMS) facility converts sample organic carbon to

185 carbon dioxide (CO₂) gas through a continuous temperature ramp, either by pyrolysis or
186 oxidation, depending on the instrument plumbing (Hemingway et al. 2017). For each
187 drying treatment, the same size subsamples across the particle sample or deployment
188 blank replicate filters were combined prior to analysis, equating to 3-5% of the active
189 sample filter area or ~9% of the deployment blank filter area. Particle sub-samples were
190 analyzed three times, resulting in three thermograms per drying treatment that recorded
191 CO₂ evolved during the temperature ramp (Fig. 2a-c). Deployment blank filters were only
192 analyzed once. Furthermore, ~5% of a pre-baked (up to 450°C) but non-deployed QMA
193 filter was also analyzed by ramped oxidation.

194 All RPO analyses were conducted following protocol described in Rosenheim et
195 al. (2008) and Hemingway et al. (2017). All filter subsamples were inserted into a quartz
196 reactor inside one of two furnaces (referred to as ovens A and B) programmed to heat at
197 5°C/minute from room temperature to 1000°C (Table 2). During the temperature ramp,
198 roughly 35 mL/min of ~92% Ultra-High Purity helium and ~8% oxygen gas flowed
199 through the quartz insert from the programmed furnace, carrying oxidation products to an
200 800°C furnace equipped with a copper, platinum and nickel catalyst that fully converts
201 the products into CO₂ gas. Consistent flow rates, He:O₂ proportions in the gas source,
202 furnace catalyst and insulation, and plumbing across RPO analyses minimized
203 instrumental variation within the data set. Downstream of the catalyst, the CO₂ and
204 carrier gas passed through a *Sable Systems*® CA-10 infrared gas analyzer, which
205 measured the outgoing CO₂ concentration, which was calibrated at 0 ppm and >400 ppm.
206 After the gas analyzer, the gas mixture flowed into a cryogenic Pyrex coil that was
207 coupled to a vacuum line, where the CO₂ gas was cryogenically trapped and released into

208 a vacuum line within user-specified temperature intervals. The gas was quantified
209 barometrically and converted to mass to calculate a carbon yield for the entire analysis.

210

211 **2.4 Compound-specific measurements**

212

213 Compound-specific abundances offer the highest resolution comparisons of
214 organic matter composition across drying treatments in this report. We limited analysis to
215 the abundances of fatty acids, sterols and alcohols, which are commonly applied to study
216 marine POC dynamics in the water column (e.g., Wakeham and Canuel 1988; Cavagna et
217 al. 2013).

218 Roughly 5% of the 125 cm² sample QMA filter active area and ~7-15% of the
219 deployment blank filter area were extracted in 15-20 mL of 9:1 dichloromethane:
220 methanol (DCM: MeOH) at 100°C for 20 minutes using a *CEMS* Corporation Microwave
221 Accelerated Reaction System. For each drying treatment, the extracts represented the
222 combined, equal sub-fractions of the three sample filters or the two blank filters collected
223 (Fig. 1). After extraction, the total lipid extract was saponified in 0.5 M potassium
224 hydroxide in MeOH for two hours at 70°C. Following saponification, liquid-liquid
225 extractions separated the basic phase from the acidic phase, each of which was eluted
226 through aminopropyl silica gel columns to separate compounds into five compound
227 classes based on their polarity. Fatty acids of both acid and base phases were recombined
228 and methylated for 12 hours at 70°C, and purified through another silica gel column prior
229 to analysis on a flame ionization detector coupled to a *Hewlett Packard 5890 Series II*
230 Gas Chromatograph (GC-FID). Sterols and alcohols of acid and base fractions were

231 acetylated separately in acetic anhydride and pyridine (1:1) for 2 hours at 70°C prior to
232 analysis on the GC-FID.

233 All sample and deployment blank analyses were accompanied by quantification of
234 synthetic standards that contained a suite of fatty acids, sterols and alcohols with known
235 concentrations and retention times. Retention times were used to identify specific
236 compounds in the samples and deployment blanks. Other compound identities,
237 particularly those of the unsaturated and branched FAMES, and gorgosterol, were
238 separately validated using an *Agilent 7890A* gas chromatograph interfaced with a
239 *Markes/Almsco BenchTOF-Select* time of flight mass spectrometer. To evaluate sample
240 drying effects on compound abundances, we directly compared peak areas across samples
241 and blanks after normalizing the areas to the fraction of QMA filter active area extracted.
242 Normalized peak abundances errors were assumed to be ~10% based on normalized peak
243 abundances from replicate analyses of the fatty acid standard. Individual peak abundance
244 errors were propagated in all subsequent analyses discussed in Section 3.3.

245

246 **3 Assessment**

247

248 The following compares the bulk, compound-specific and thermal composition of
249 marine POC collected from the coastal waters of Woods Hole, MA and treated by oven-
250 drying, air-drying or freeze-drying. To interpret thermal stability, we assume that
251 biomolecules in an organic matrix span a range of activation energies of decomposition
252 (Cramer 2004; Rosenheim et al. 2008; Rosenheim and Galy 2012; Rosenheim et al.
253 2013), which would drive differences in the oxidation temperature of compounds and

254 fragments of compounds during ramped oxidation. Our interpretations of bulk carbon
255 composition and thermal stability rely on the assumption that PIC concentrations in
256 particulate matter are negligible, and that the carbon quantities reported correspond
257 predominantly to organic carbon in the samples. The consistently depleted isotope
258 composition of the bulk carbon corroborates this assumption (Table 1). This is further
259 reflected by the lack of any significant calcifying organisms observed on SEM images of
260 particle sample QMA filters (Fig. 1c).

261

262 **3.1 Invariant bulk composition across drying treatments**

263

264 All carbon and nitrogen quantities measured on three sample QMA filters (one
265 per drying treatment) and one deployment blank filter (freeze-dried only) were
266 normalized to the total active area of the filter (125 cm²) and volume filtered, yielding
267 total C and N filter loadings and concentrations, respectively (Table 1). Particle sample C
268 loadings ranged from 10.5 - 13.2 mg C/QMA, corresponding to 11.9 - 16.7 μM C. Total
269 N concentrations ranged from 1.8 - 2.5 μM. Because the bulk measurements were
270 conducted on individual filter samples (Section 2.2), variability between McLane pump
271 deployments and environmental heterogeneity of the particle pool drive the range in the
272 total carbon and nitrogen loadings on the QMA filters, in addition to any effects imposed
273 by the different drying treatments.

274 More importantly, despite these differences in the carbon loading among the
275 particle sample filters, relatively invariant bulk $\delta^{13}\text{C}$, $\delta^{15}\text{N}$ and C/N values across filters
276 from different treatments and deployments imply that air-drying and oven-drying do not

277 appreciably affect bulk POC composition relative to freeze-drying (Table 1). Bulk $\delta^{13}\text{C}$
278 values of sample carbon ranged from -23.9 ‰ to -23.6 ‰, $\delta^{15}\text{N}$ values ranged from 7.9‰
279 to 8.3 ‰, and C/N values ranged from 6.5 - 6.8. The standard deviation of the three $\delta^{13}\text{C}$
280 (± 0.1 ‰), $\delta^{15}\text{N}$ (± 0.2 ‰) and C/N (± 0.2 $\mu\text{mol}/\mu\text{mol}$) values measured across sample
281 filters are comparable to or smaller than the analytical precision of each measurement.

282 The total carbon and nitrogen loadings on the freeze-dried deployment blank filter
283 sub-sample were 10-20 times lower than the bulk content on the three particle sample
284 filters analyzed (Table 1). The $\delta^{13}\text{C}$ of the blank carbon was -25.6 ‰, ~ 2 ‰ more
285 depleted than the $\delta^{13}\text{C}$ values of the particle samples. At the same time, the scanning
286 electron images of the deployment blank filters showed no evidence of particles on the
287 filter fibers (Fig. 1b), consistent with the assumption that the small quantity of carbon on
288 the deployment blank filters is likely sorbed dissolved organic carbon.

289

290 **3.2 Thermal stability not affected by drying treatments**

291

292 All < 51 μm combined particle samples and deployment blanks, oven-dried, air-
293 dried and freeze-dried, were analyzed by ramped oxidation between 100°C and 1000°C,
294 with most sample and blank carbon oxidizing between 150°C and 600°C (Fig. 2). In
295 general, the total CO_2 gas evolved during ramped oxidation of each combined particle
296 sample and blank, barometrically quantified in the vacuum line and normalized to the 125
297 cm^2 active area of a QMA filter, served as an estimate of the total sample carbon
298 integrated across all different filter deployments treated by the same drying process

299 (Table 2). The exception was the second freeze-dried sample run, for which no CO₂
300 pressure was quantified and converted to a total carbon yield.

301 The deployment blank RPO analyses provide further evidence for organic carbon
302 sorption onto QMA filters. Thermograms of combined deployment blanks yielded 0.5 -
303 1.1 mg carbon/filter across drying treatments (Table 2, Fig. 2d), 3-10 times greater than
304 the carbon yielded from a pre-combusted unused blank QMA (Fig. 2e), and several
305 orders of magnitude higher than the estimated blank contribution for the NOSAMS RPO
306 system (Hemingway et al. 2017). Carbon yields from the deployment blank analyses
307 were not significantly different across drying treatments, considering that replicate
308 ramped oxidation analyses of the same size sub-sample can vary by as much as 0.07 mg
309 carbon, which exceeds differences among the relatively small carbon quantities yielded
310 during the three deployment blank analyses, pre-normalization (Table 2). Because the
311 amount of carbon on the deployment blank filters represents <10% of the total carbon
312 yield from the combined particle sample RPO analyses, and did not vary significantly
313 among drying treatments, it was not necessary to apply a blank subtraction to the particle
314 sample thermograms in this study.

315 Compared to the bulk analyses, the RPO carbon yields from the combined particle
316 sample analyses represent the average of three deployed filter samples or two deployed
317 blank replicates, and thus remove the influence of environmental heterogeneity
318 associated with different pump deployments and uneven particle loading. Differences in
319 filter area-normalized carbon yields across drying treatments are comparable to the
320 differences among replicate RPO analyses of the same sample, indicating that oven-

321 drying and air-drying do not influence the total carbon loaded on the filters relative to
322 freeze-drying (Table 2; Fig. 2a-c).

323 Similarly, the differences in thermogram shape of combined particle samples
324 across drying treatments are comparable to and do not exceed the differences among
325 triplicate thermograms of samples with the same drying treatment (Fig. 2a-c), suggesting
326 that air-drying and oven-drying do not significantly change the thermal stability of the
327 POC relative to freeze-drying. Use of different programmable ovens could account for
328 some of the smaller differences among the thermogram shapes across triplicate ramped
329 oxidation analyses of the same sample, particularly for the shifts along the temperature
330 axis. Thermograms of replicate sample analyses using the same oven, Oven A (Fig. 2f),
331 line up better in temperature space than repeated analyses of the same sample using two
332 different ovens, Ovens A and B (Figs. 2a-c). In the future, periodically running standard
333 compounds with well-defined peaks, such as sodium bicarbonate, in the different sample
334 ovens would help normalize these temperature shifts in thermograms generated by
335 different ovens (Rosenheim et al. 2008).

336

337 **3.3 Drying temperature alters lipid composition**

338

339 Abundances of fatty acids, sterols and alcohols in combined particle samples and
340 deployment blanks were quantified across a range of molecular sizes. Peaks from each
341 particle sample and deployment blank chromatogram represented an average of the
342 different replicate filters deployed (Section 2.4). The areas of select compound peaks
343 were normalized to the area of an entire QMA filter (Table S1). Next, for each drying

344 treatment, filter-normalized peak areas across the deployment blank chromatograms were
345 subtracted from matching filter-normalized peak areas in the sample chromatograms.
346 Finally, we compared ratios of each normalized and blank-corrected peak area in the
347 oven-dried (“O”) and air-dried (“A”) combined particle samples to corresponding
348 normalized and blank-corrected peak areas in the freeze-dried sample (“F”). For the rest
349 of the discussion, these ratios are $R_{O/F}$ and $R_{A/F}$, respectively. Ratios less than one
350 indicate depression of compound abundances in oven-dried or air-dried samples relative
351 to compound abundances in freeze-dried samples.

352 Unlike the bulk and ramped oxidation data, the lipid analyses imply that oven-
353 and air-drying affected compounds associated with the deployment blank filters
354 differently than they affected the same compounds in the particulate carbon pool. Indeed,
355 for most compounds, $R_{O/F}$ and $R_{A/F}$ ratios in deployment blanks deviated from
356 corresponding ratios in the combined particle samples (Figs. 3c, 4c, 5c; Table S1). For
357 this reason, we applied a blank correction to particle sample abundances to better control
358 for differences between drying effects on the sorbed lipid pool and drying effects on
359 particulate lipid pool. The processes decoupling the sorbed lipid pool from the
360 particulate lipid pool, unlikely to result from methodological errors in sample preparation
361 or contamination of the deployment blank filters, are beyond the scope of this study.

362 Fatty acid analysis spanned a range of molecular sizes, including saturated
363 straight-chain fatty acids (12 to 24 carbon chain lengths, or C_{12} - C_{24}), straight-chain
364 unsaturated fatty acids (C_{14} - C_{22}), and saturated branched fatty acids produced by bacteria
365 (C_{15} , C_{16} , C_{17}). Calculated $R_{O/F}$ and $R_{A/F}$ values for fatty acids were consistently below 1
366 (Figs. 3-5), indicating that these compounds are less abundant in the oven-dried and air-

367 dried samples relative to the freeze-dried samples. The $R_{O/F}$ values were generally lower
368 than the $R_{A/F}$ values for the same compounds, especially among the straight-chain and
369 branched saturated fatty acids (Figs. 3c, 5a-b). Calculated $R_{O/F}$ and $R_{A/F}$ values among
370 saturated straight-chain fatty acids correlate positively with the carbon chain length of the
371 compound ($p < 0.05$) (Fig. 3a, b). The correlation between $R_{A/F}$ and chain length is
372 stronger (Fig. 3b) than the correlation between $R_{O/F}$ and chain length (Fig. 3a), which is
373 reflected in a steeper slope of the best linear fit and a higher R^2 value. Relatedly, $R_{A/F}$ and
374 $R_{O/F}$ values are similar at lower molecular weights and diverge at higher molecular
375 weights, with $R_{A/F}$ values consistently higher (closer to a value of 1) than $R_{O/F}$ values.
376 The greater overall depression in fatty acid abundances as a result of oven-drying
377 suggests that physical mechanisms like volatilization, which depends upon chain length
378 and molar mass, play an important role in the effects of drying treatment on straight-
379 chain saturated fatty acid abundances (Meylan and Howard 1991; Lide 1996; Daubert
380 1997; Schwarzenbach et al. 2003). Thus, drying temperatures can influence the
381 distribution of fatty acids in a sample by driving differential loss of compounds with
382 varying molecular weights and volatility.

383 There is no clear relationship between chain length and $R_{O/F}$ and $R_{A/F}$ values for
384 unsaturated straight-chain and saturated branched fatty acids quantified across samples,
385 as they are relatively invariant and below 1 across chain lengths (Figs. 4, 5). Among the
386 straight-chain unsaturated fatty acids, ratios tend to decrease with increasing numbers of
387 non-single bonds, indicating that compounds with higher degrees of unsaturation are less
388 physically stable and therefore more sensitive to the effects of air-drying and oven-drying
389 (Lide 1996; Schwarzenbach et al. 2003).

390 Specific alcohols and sterols were identified using a suite of seven standard
391 compounds with different molar masses, carbon chain lengths and environmental origins
392 (Table 3). Calculated $R_{O/F}$ values across blank-corrected samples were lowest (0.57) for
393 gorgosterol, as high as 1.3 for 1-hexadecanol, and averaged at 0.97 ± 0.22 across all
394 compounds (Table 3, Fig. 6a). Calculated $R_{A/F}$ values were 0.86 ± 0.09 (mean \pm 1 S.D.),
395 lowest for gorgosterol (0.68), and highest for 5α -cholestan- 3β -ol (0.97) (Fig. 6b).
396 Compared to fatty acid abundances, peak areas of seven sterols and alcohols quantified
397 across the combined particle samples shifted less as a result of different drying
398 treatments. $R_{O/F}$ and $R_{A/F}$ values for all compounds except gorgosterol ranged from 0.83
399 to 1.3 (Fig. 6a-b). These diminished effects may, in part, result from lower vapor
400 pressures associated with sterol compounds relative to fatty acids (Meylan and Howard
401 1991). Only abundances of gorgosterol in the oven-dried and air-dried samples were
402 anomalously depressed (<0.7), while the abundance of 1-hexadecanol in the oven-dried
403 sample was anomalously elevated (>1.25).

404 The anomalously high 1-hexadecanol ratio in the oven-dried combined particle
405 sample may be an artifact of uneven blank subtractions across drying treatments, a
406 proportionally greater subtraction in the freeze-dried sample than in the oven-dried
407 sample (Table S1). In general, blank corrections for other compounds that are similarly
408 abundant in the deployment blank relative to the particle samples could bias the results
409 presented here. Fortunately, lipid abundance comparisons without a blank subtraction do
410 not greatly differ from and in some cases strengthen interpretations based on an initial
411 blank subtraction (Fig. 6). For example, $R_{O/F}$ and $R_{A/F}$ values for sterols/alcohols
412 including 1-hexadecanol prior to blank correction are much closer to 1.0 and much less

413 variable across molecular weights (Fig. 6d-e), strengthening the argument that different
414 drying treatments affect alcohol and sterol abundances less than they affect fatty acid
415 abundances.

416 Overall, the fact that oven-drying and air-drying shift specific lipid abundances
417 according to their physical properties (e.g., molecular weight and structure), while bulk
418 characteristics and thermal stability remain unaffected across treatments, supports the
419 argument that sample treatment effects are abiotic rather than mediated by biological
420 activity. These drying processes may impose enough heat or airflow to physically remove
421 some of the light-weight, more volatile molecules. Further, we argue that effects from
422 two other processes that shift the abundance distributions of lipids in field samples,
423 bacterial degradation (Wakeham and Volkman 1991; Ohman 1996; Wakeham et al.
424 2002) and abiotic oxidation (Wang et al. 2017), are unlikely here. The relatively
425 depressed branched fatty acid abundances, which derive from bacteria, in the oven-dried
426 and air-dried samples (Fig. 5) indicate that the drying period (<24 hours) for the oven-
427 dried and air-dried samples was likely short enough to limit any significant alteration by
428 heterotrophic activity. Further, Wang et al. (2017) observed that oxidative breakdown of
429 higher chain-length *n*-alkanes at temperatures as low as 60°C generated lower chain-
430 length *n*-alkane by-products, shifting the lipid distribution in soils collected from the
431 field. Our lipid data set does not support this process, exhibiting the reverse relationship
432 between chain length and straight-chain saturated fatty acid abundances and no
433 relationship between chain length and straight-chain unsaturated/branched saturated fatty
434 acid abundances.

435

436 **4 Discussion**

437

438 The bulk and ramped oxidation analyses of particle samples suggest that
439 preservation of marine POC from the field by oven and air-drying does not compromise
440 the bulk isotope composition, bulk C/N and thermal stability of the sample compared to
441 storage at -80°C and freeze-drying. Thus, samples dried quickly, i.e., in less than 24
442 hours, at temperatures between 25°C and 56°C, can still be characterized by these
443 metrics. By contrast, filter-normalized and blank-corrected abundances of extracted lipids
444 across POC samples show that oven-drying and air-drying do shift lipid abundances, and
445 that the magnitude of this shift depends on compound structure and molecular size. These
446 results generally agree with prior research demonstrating that warmer sample storage
447 temperatures differentially compromise distinct lipid classes (Ohman 1996). But, this
448 study expands our understanding of temperature effects on POC sample preservation by
449 directly investigating the impact of different drying temperatures rather than different
450 storage temperatures. Unlike earlier studies, this assessment shows that the differences in
451 lipid composition among drying treatments over shorter time scales of less than one day
452 derive from abiotic processes like compound volatilization, rather than biotic processes
453 like enzymatic or heterotrophic degradation, which may be more important when
454 considering wet storage of samples above -80°C.

455 Typically, lipids make up at most 25% of total biomass in living microalgae
456 (Finkel et al. 2016), which are the primary producers of POC in the shallow, coastal
457 waters of Woods Hole in June. In this study, we have monitored only a small fraction of
458 the marine lipid pool (Wakeham and Volkman 1991), and have found that some

459 compounds are as much as ~90% depleted in non-freeze-dried samples relative to freeze-
460 dried samples. More than 50% of several of these compounds, however, are still present
461 in oven-dried and air-dried sample POC relative to freeze-dried POC. Taken together,
462 such shifts in compound-specific abundances as a result of different drying treatments
463 must be small relative to the bulk organic matter composition, as bulk $\delta^{13}\text{C}$, $\delta^{15}\text{N}$, C/N
464 and thermal stability do not vary across drying treatments.

465

466 **5 Comments and recommendations**

467

468 The results of this sample treatment comparison highlight several characteristics
469 of POC composition (bulk C/N, $\delta^{13}\text{C}$, $\delta^{15}\text{N}$, and thermal stability) that are not
470 compromised by oven-drying at 56°C or air-drying at high flow and room temperature
471 when the particle samples are dried within 24 hours following collection. As this
472 approach to sample treatment is common in the field (e.g., Buesseler et al. 2005; Bishop
473 and Wood 2008; Bishop et al. 2012; Lam et al. 2015; Rosengard et al. 2015), these
474 findings imply that a vast repository of marine particle samples collected at sea remain
475 useful tracers of POC composition and cycling in the water column, even if originally
476 unintended for such research questions at the time of collection. These particle samples
477 collected and processed by such drying treatments may still be used for bulk organic
478 analysis and ramped pyrolysis/oxidation, the latter of which will expand the empirical
479 applications of this method to understanding marine POC dynamics in the water column.

480 At the same time, these samples are not appropriate for lipid analysis. Oven-
481 drying and air-drying do shift the lipid distribution and potentially the distribution of

482 other compound classes in organic matter. The magnitude of these effects on compound
483 class abundances are overwhelmed by a greater proportion of unaltered material in the
484 bulk carbon pool. The data here do not shed light on how the compound-specific stable
485 carbon isotope composition of these compound classes may be altered by oven-drying or
486 air-drying, i.e., whether there is a fractionation effect associated with molecular
487 volatilization of compounds off of QMA filters during the drying process (Wang et al.
488 2017). Furthermore, this report does not suggest that slower flow air-drying at room
489 temperature, rather than higher flow air, would similarly conserve the bulk and thermal
490 stability properties of POC. These uncertainties would be appropriate for future studies
491 with a comparably controlled approach.

492

493

494 **References**

495

- 496 Bishop, J. K., P. J. Lam, and T. J. Wood. 2012. Getting good particles: Accurate
497 sampling of particles by large volume in-situ filtration. *Limnol. Oceanogr.*
498 *Methods* **10**: 681-710.
- 499 Bishop, J. K. B., and T. J. Wood. 2008. Particulate matter chemistry and dynamics in the
500 twilight zone at VERTIGO ALOHA and K2 sites. *Deep Sea Research Part I:*
501 *Oceanographic Research Papers* **55**: 1684-1706.
- 502 Buesseler, K. O., J. E. Andrews, S. M. Pike, M. A. Charette, L. E. Goldson, M. A.
503 Brzezinski, and V. P. Lance. 2005. Particle export during the southern ocean iron
504 experiment (SOFeX). *Limnology and Oceanography* **50**: 311-327.
- 505 Burd, A. B., S. Frey, A. Cabre, and others. 2016. Terrestrial and marine perspectives on
506 modeling organic matter degradation pathways. *Global Change Biology* **22**: 121-
507 136.
- 508 Burdige, D. J. 2007. Preservation of Organic Matter in Marine Sediments: Controls,
509 Mechanisms, and an Imbalance in Sediment Organic Carbon Budgets? *Chemical*
510 *Reviews* **107**: 467-485.
- 511 Cavagna, A.-J., F. Dehairs, S. Bouillon, V. Woule-Ebongué, F. Planchon, B. Delille, I.
512 Bouloubassi. 2013. Water column distribution and carbon isotopic signal of
513 cholesterol, brassicasterol and particulate organic carbon in the Atlantic sector of
514 the Southern Ocean. *Biogeosciences* **10**: 2787-2801.
- 515 Cramer, B. 2004. Methane generation from coal during open system pyrolysis
516 investigated by isotope specific, Gaussian distributed reaction kinetics. *Organic*
517 *Geochemistry* **35**: 379-392.
- 518 Daubert, T. 1997. Physical and thermodynamic properties of pure chemicals, National
519 Standard Reference Data System. American Institute of Chemical Engineering.
- 520 Finkel, Z. V., M. J. Follows, J. D. Liefer, C. M. Brown, I. Benner, and A. J. Irwin. 2016.
521 Phylogenetic Diversity in the Macromolecular Composition of Microalgae. *PloS*
522 *one* **11**.
- 523 Francois, R., S. Honjo, R. Krishfield, and S. Manganini. 2002. Factors controlling the
524 flux of organic carbon to the bathypelagic zone of the ocean. *Global*
525 *Biogeochemical Cycles* **16**: doi:10.1029/2001GB001722.
- 526 Grimalt, J. O., E. Torras, and J. Albaigés. 1988. Bacterial reworking of sedimentary lipids
527 during sample storage. *Organic Geochemistry* **13**: 741-746.
- 528 Hemingway, J. D., V. V. Galy, A. R. Gagnon, K. E. Grant, S. Z. Rosengard, G. Soulet, P.
529 K. Zigah, and A. P. McNichol. 2017. Assessing the Blank Carbon Contribution,
530 Isotope Mass Balance, and Kinetic Isotope Fractionation of the Ramped
531 Pyrolysis/Oxidation Instrument at NOSAMS. *Radiocarbon* **59**: 179-193.
- 532 Kaehler, S., and E. Pakhomov. 2001. Effects of storage and preservation on the d13C and
533 d15N signatures of selected marine organisms. *Marine Ecology Progress Series*
534 **219**: 299-304.
- 535 Lam, P. J., D. C. Ohnemus, and M. E. Auro. 2015. Size-fractionated major particle
536 composition and concentrations from the US GEOTRACES north Atlantic zonal

537 transect. *Deep Sea Research Part II: Topical Studies in Oceanography* **116**: 303-
538 320.

539 Lide, D. R. 1996. *Handbook of Chemistry and Physics: CRC Handbook*. CRC Press.

540 Meylan, W. M., and P. H. Howard. 1991. Bond contribution method for estimating
541 Henry's law constants. *Environmental toxicology and chemistry* **10**: 1283-1293.

542 Ohman, M. 1996. Freezing and storage of copepod samples for the analysis of lipids.
543 *Marine ecology progress series* **130**: 295-298.

544 Repeta, D. J. 2014. Chemical characterization and cycling of dissolved organic matter, p.
545 21–63. In D. A. Hansell and C. A. Carlson [eds.], *Biogeochemistry of marine*
546 *dissolved organic matter*. Elsevier.

547 Rosengard, S. Z., P. J. Lam, W. M. Balch, M. E. Auro, S. Pike, D. Drapeau, and B.
548 Bowler. 2015. Carbon export and transfer to depth across the Southern Ocean
549 Great Calcite Belt. *Biogeosciences* **12**: 3953-3971.

550 Rosenheim, B. E., M. B. Day, E. Domack, H. Schrum, A. Benthien, and J. M. Hayes.
551 2008. Antarctic sediment chronology by programmed-temperature pyrolysis:
552 Methodology and data treatment. *Geochem. Geophys. Geosyst.* **9**: Q04005.
553 doi:[10.1029/2007GC001816](https://doi.org/10.1029/2007GC001816)

554 Rosenheim, B. E., and V. Galy. 2012. Direct measurement of riverine particulate organic
555 carbon age structure. *Geophys. Res. Lett.* **39**: L19703.
556 doi:[10.1029/2012GL052883](https://doi.org/10.1029/2012GL052883)

557 Rosenheim, B. E., K. M. Roe, B. J. Roberts, A. S. Kolker, M. A. Allison, and K. H.
558 Johannesson. 2013. River discharge influences on particulate organic carbon age
559 structure in the Mississippi/Atchafalaya River System. *Global Biogeochem.*
560 *Cycles* **27**: 154–166. doi:[10.1002/gbc.20018](https://doi.org/10.1002/gbc.20018)

561 Schwarzenbach, R. P., P. M. Gschwend, and D. M. Imboden. 2003. *Environmental*
562 *organic chemistry*. John Wiley & Sons.

563 Subt, C., K. A. Fangman, J. S. Wellner, and B. E. Rosenheim. 2016. Sediment
564 chronology in Antarctic deglacial sediments: Reconciling organic carbon 14C
565 ages to carbonate 14C ages using Ramped PyrOx. *The Holocene* **26**: 265-273.

566 Trull, T., and L. Armand. 2001. Insights into Southern Ocean carbon export from the
567 $\delta^{13}\text{C}$ of particles and dissolved inorganic carbon during the SOIREE iron release
568 experiment. *Deep Sea Research Part II: Topical Studies in Oceanography* **48**:
569 2655-2680.

570 Wagner, B. A., G. R. Buettner, and C. P. Burns. 1994. Free Radical-Mediated Lipid
571 Peroxidation in Cells: Oxidizability Is a Function of Cell Lipid bis-Allylic
572 Hydrogen Content. *Biochemistry* **33**: 4449-4453.

573 Wakeham, S. G., and E. A. Canuel. 1988. Organic geochemistry of particulate matter in
574 the eastern tropical North Pacific Ocean: Implications for particle dynamics.
575 *Journal of Marine Research* **46**: 183-213.

576 Wakeham, S. G., M. L. Peterson, J. I. Hedges, and C. Lee. 2002. Lipid biomarker fluxes
577 in the Arabian Sea, with a comparison to the equatorial Pacific Ocean. *Deep-Sea*
578 *Research Part Ii-Topical Studies in Oceanography* **49**: 2265-2301.

579 Wakeham, S. G., and J. K. Volkman. 1991. Sampling and analysis of lipids in marine
580 particulate matter, p. 171–179. In D. C. Hurd and D. W. Spencer [eds.], *Marine*
581 *particles: Analysis and characterization*. American Geophysical Union.

582 Wang, C., Y. Eley, A. Oakes, and M. Hren. 2017. Hydrogen isotope and molecular

583
584

alteration of n-alkanes during heating in open and closed systems. *Org. Geochem.*
112: 47–58. doi:[10.1016/j.orggeochem.2017.07.006](https://doi.org/10.1016/j.orggeochem.2017.07.006)

585 Table 1. The bulk composition of <51 μm particulate organic matter loaded onto three sample and two blank <51 μm QMA filters
 586 (active area $\sim 125 \text{ cm}^2$) that were either dried in an oven, laminar flow hood or freeze-dried. Filters were divided into thirds prior to
 587 drying so that each treatment could be applied to each blank or sample filter. Sub-samples from individual thirds of different McLane
 588 pump deployments were analyzed for bulk composition. Particle sample values here were not blank-corrected.

589

Sample	Deployment	Volume (L)	Treatment	C/filter*	[C]*	[N]*	C/N	$\delta^{13}\text{C}$	$\delta^{15}\text{N}$
--	--	<i>L</i>	--	<i>mg/filter</i>	μM	μM	$\mu\text{mol}/\mu\text{mol}$	‰	‰
POC1	1	95.4	oven-dried						
POC1	1	95.4	air-dried	14	12.4	1.9	6.5	-23.6	7.9
POC1	1	95.4	freeze-dried						
POC2	1	93.8	oven-dried						
POC2	1	93.8	air-dried						
POC2	1	93.8	freeze-dried	13	11.9	1.8	6.8	-23.9	8.3
POC3	2	40.5	oven-dried	8	16.7	2.5	6.8	-23.8	8.2
POC3	2	40.5	air-dried						
POC3	2	40.5	freeze-dried						
db1	1	0	oven-dried						
db1	1	0	air-dried						
db1	1	0	freeze-dried	0.7	N/A	N/A	7.7	-25.6	BDL
db2	2	0	oven-dried						
db2	2	0	air-dried						
db2	2	0	freeze-dried						

590
 591
 592
 593

BDL= below detection limit.

“db”= deployment blank.

*quantities are normalized to active area of the QMA filter, 125 cm^2

594 Table 2. Carbon released per analysis and filter-normalized carbon yields calculated from
 595 ramped oxidation of sample and deployment blank filters. No CO₂ quantities were
 596 measured and converted to carbon mass during the second freeze-dried sample analysis.
 597 Carbon values reported here were not blank-corrected.

598

Sample Type	Treatment	Analysis #	Oven	mg C/analysis	Fraction of OMA analyzed	mg C/filter (125 cm ²)	
POC1+2+3	Oven-dried	I	A	0.697	5%	12.8	
POC1+2+3	Oven-dried	II	A	0.337	3%	12.4	Mean ± S.D.
POC1+2+3	Oven-dried	III	B	0.346	3%	12.7	12.6 ± 0.2
POC1+2+3	Air-dried	I	A	0.678	5%	12.5	
POC1+2+3	Air-dried	II	B	0.352	3%	12.9	Mean ± S.D.
POC1+2+3	Air-dried	III	B	0.286	3%	10.5	12.0 ± 1.3
POC1+2+3	Freeze-dried	I	A	0.721	5%	13.2	
POC1+2+3	Freeze-dried	II	B	no data	3%	no data	
POC1+2+3	Freeze-dried	III	B	0.314	3%	11.5	
db1+2	Oven-dried	I	A	0.050	9%	0.5	
db1+2	Air-dried	I	A	0.042	9%	0.5	Mean ± S.D.
db1+2	Freeze-dried	I	A	0.104	9%	1.1	0.7 ± 0.4

599

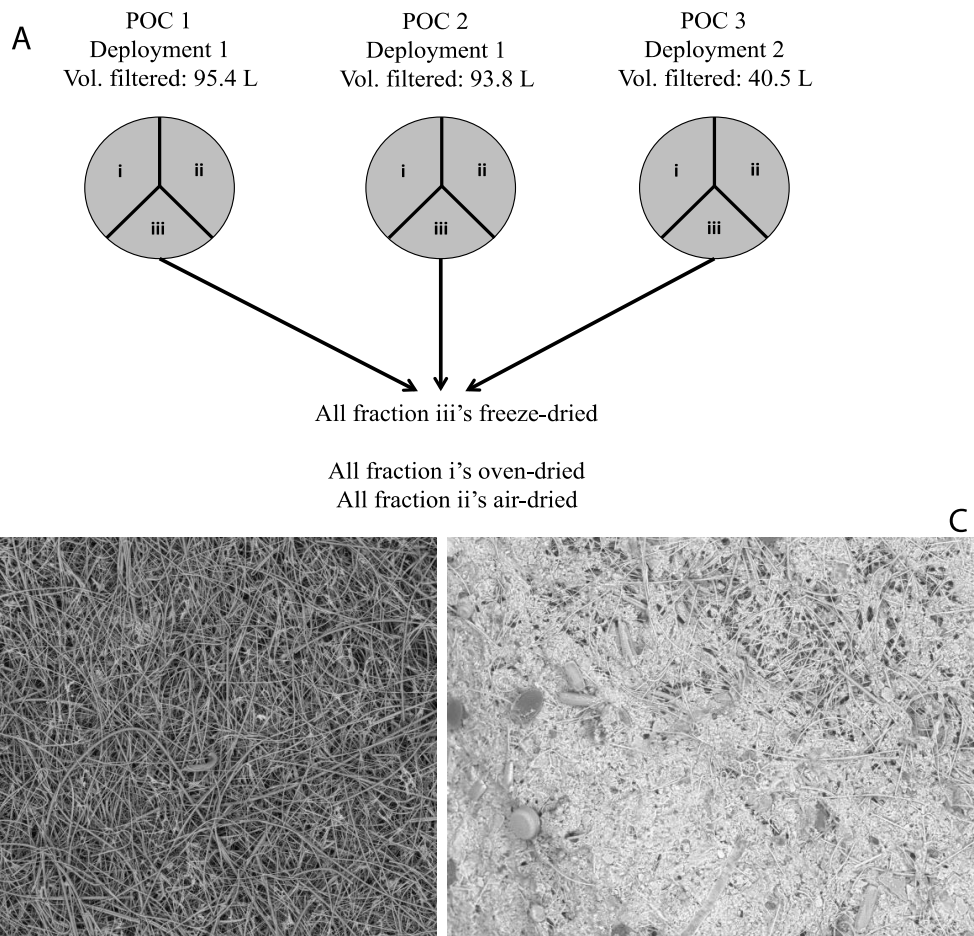
“db”=deployment blank

600 Table 3. Constituents of the alcohol/sterol standards and their properties.

601

Standard compound	Class	Molar Mass	# Carbon	Known sources
--	--	<i>g/mol</i>	<i>#</i>	--
Phytol	Alcohol	196.539	20	Chlorophyll
1-hexadecanol	Alcohol	242.447	16	Ubiquitous
Cholesterol	Sterol	386.664	27	Ubiquitous
5 α -cholestan-3 β -ol	Sterol	388.68	27	Cholesterol derivative in biological matter
Brassicasterol	Sterol	398.675	28	Unicellular algae, some terrestrial plants
Stigmasterol	Sterol	412.702	29	Terrestrial vegetation
Gorgosterol	Sterol	426.729	30	Marine algae

602



603

604 Figure 1. (a) Schematic of dock sample collection and post-processing before analysis. A

605 similar approach was used to apportion the two deployment blank filters by drying

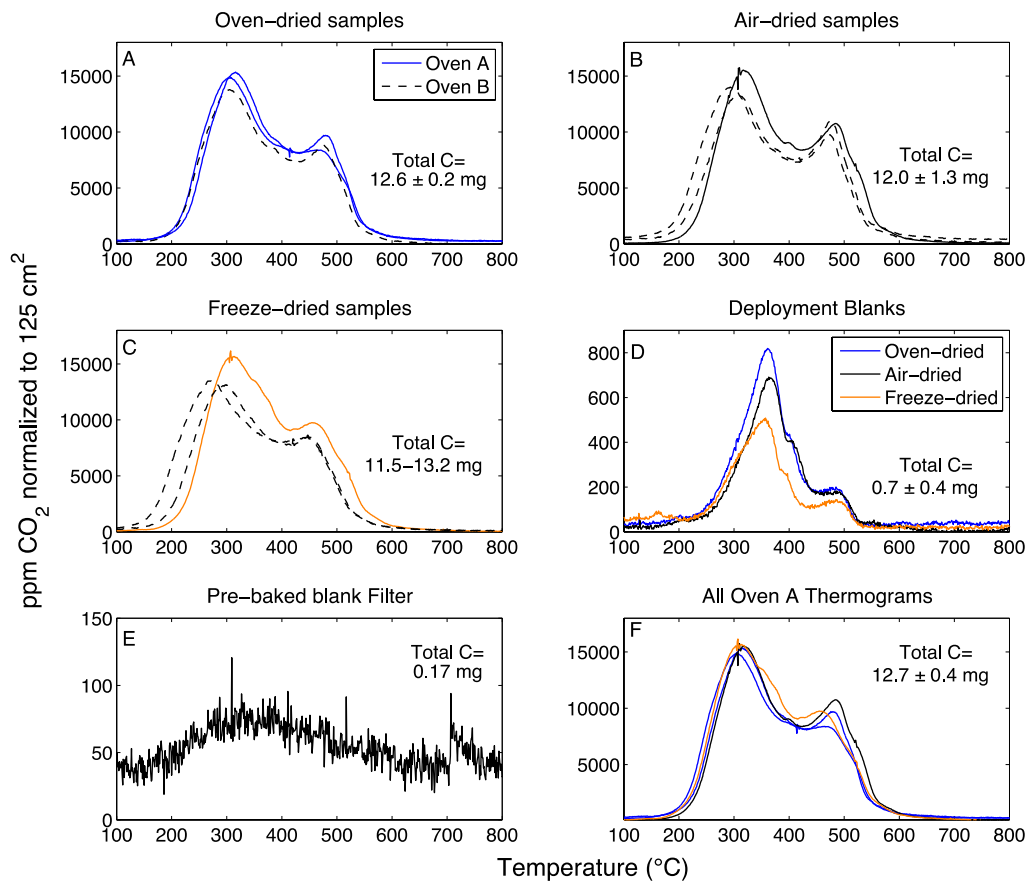
606 treatment. (b-c) Scanning electron microscope images of freeze-dried (b) deployment

607 blank and (c) sample particle filters. The images in b-c are ~0.6 cm wide. Total filter

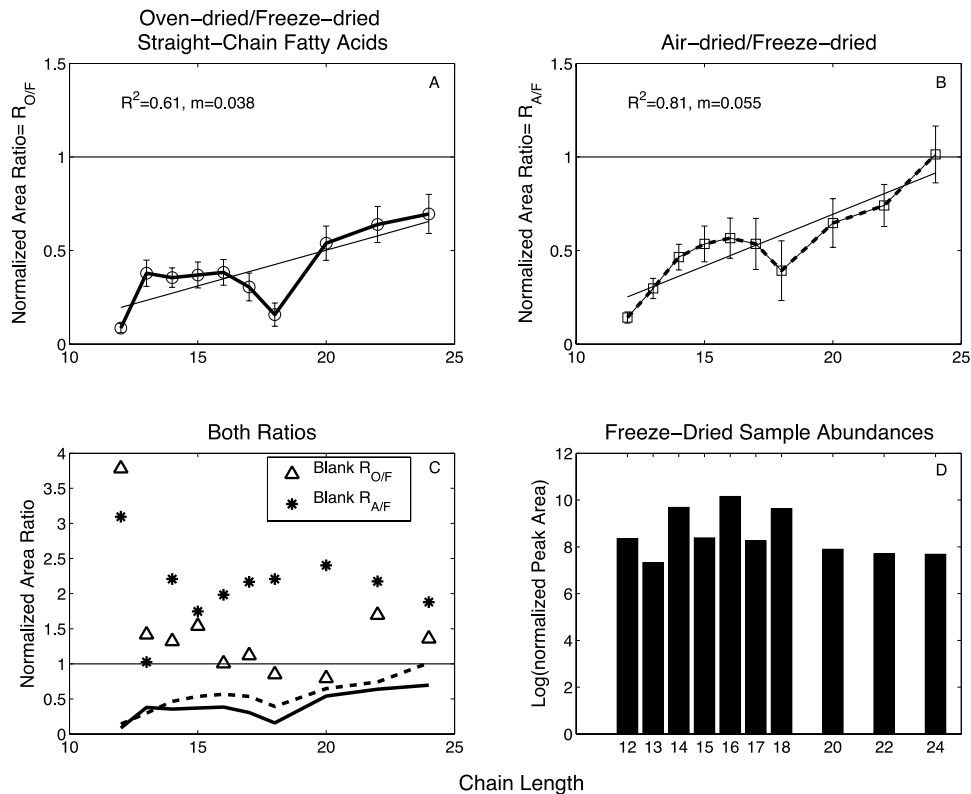
608 active area is 125cm², corresponding to a ~12.6 cm diameter.

609

610



611
 612 Figure 2. (a-c) Thermograms of combined particle sample filters generated by ramped
 613 oxidation, with replicate analyses plotted as solid colored lines (either blue, black or
 614 orange) when using furnace A vs. black dashed lines when using oven B. (d)
 615 Thermograms of deployment blanks, analyzed once per drying treatment in oven A. (e)
 616 Thermogram of a pre-combusted non-deployed QMA filter, also analyzed using oven A.
 617 (f) All sample particle thermograms analyzed in oven A. The legend in (d) applies to (f).
 618
 619



620
621 Figure 3. (a-c) Ratios of filter-normalized and blank-corrected peak areas of straight-
622 chain saturated fatty acids in (a) oven-dried particle samples relative to freeze-dried
623 samples ($R_{O/F}$) and in (b) air-dried samples relative to freeze-dried samples ($R_{A/F}$). These
624 ratios correlate significantly with compound carbon chain length ($p < 0.05$). R^2 and the
625 slope (m) values of each correlation are reported. Errors for each ratio were calculated by
626 propagating errors for filter-normalized peak abundances ($\sim 10\%$). (c) $R_{O/F}$ and $R_{A/F}$
627 plotted on the same axes, along with ratios of oven-dried (triangle) or air-dried (star)
628 blank compound abundances to freeze-dried blank compound abundances. The relative
629 errors of these ratios in the deployment blanks are $< 1\%$ and thus not shown. (d) Absolute
630 normalized and blank-corrected peak areas in the freeze-dried samples.
631

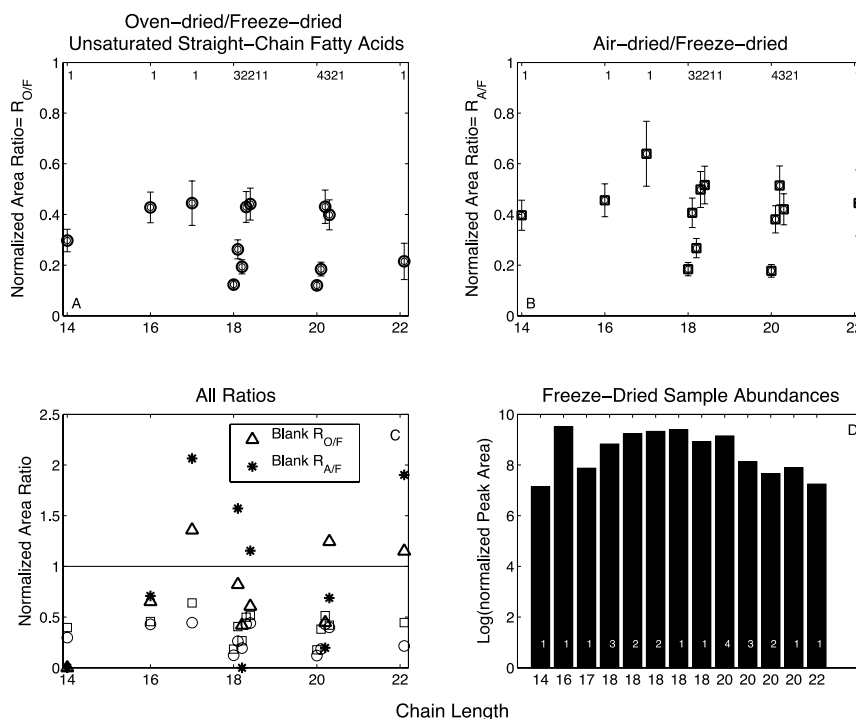
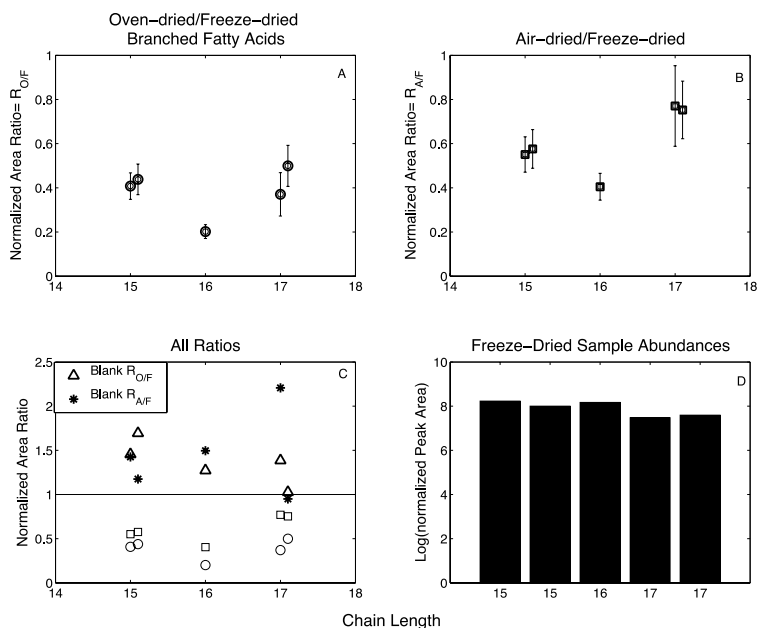


Figure 4.

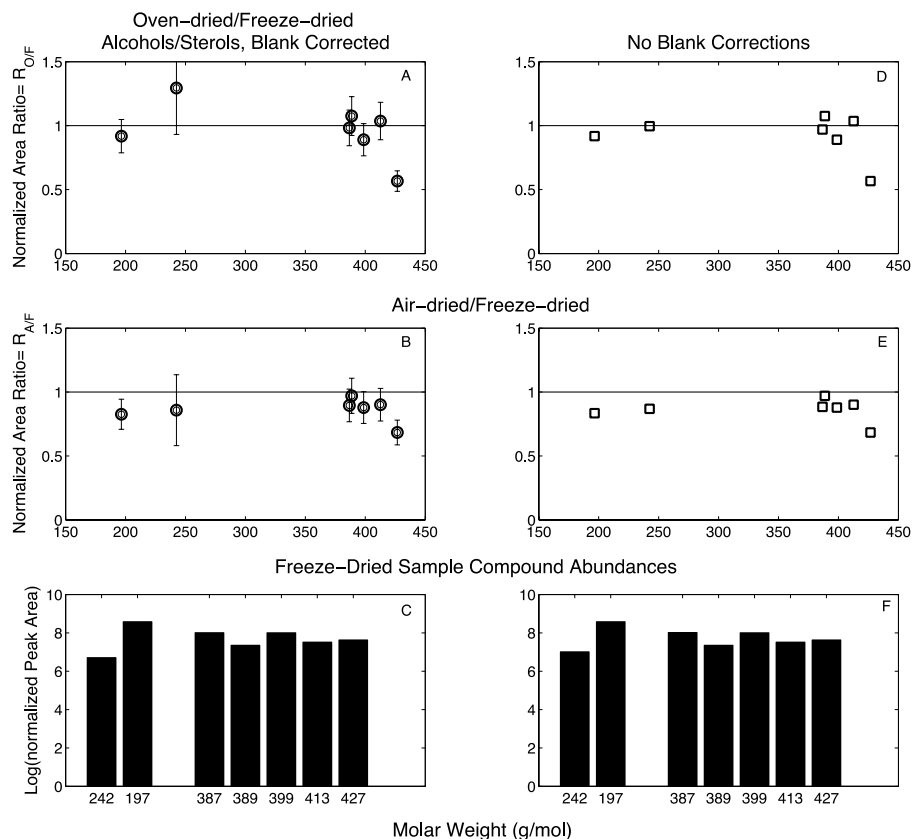
632

633 (a-b) Ratios of filter-normalized and blank-corrected peak areas of straight-chain
 634 unsaturated fatty acids in (a) oven-dried particle samples relative to freeze-dried samples
 635 ($R_{O/F}$) and in (b) air-dried samples relative to freeze-dried samples ($R_{A/F}$). Errors for each
 636 ratio were calculated by propagating errors for filter-normalized peak abundances
 637 (~10%). The numbers on the panels indicate the degrees of unsaturation, or number of
 638 non-single bonds, for compounds plotted that have the same carbon chain length. For
 639 example, the cluster of four data points around chain length 20 refers to a 20-carbon fatty
 640 acid with one to four non-single bonds. (c) $R_{O/F}$ and $R_{A/F}$ plotted on the same axes
 641 alongside ratios of oven-dried (triangle) or air-dried (star) blank compound abundances to
 642 freeze-dried blank compound abundances. The relative errors of these ratios in the
 643 deployment blanks are <1% and are thus not shown. (d) Absolute normalized and blank-
 644 corrected peak areas in the freeze-dried samples ordered by chain length. The bars are
 645 labeled by the number of non-single bonds in the compound plotted.



646

647 Figure 5. (a-b) Ratios of filter-normalized and blank-corrected peak areas of three
 648 branched saturated fatty acids in (a) oven-dried particle samples relative to freeze-dried
 649 samples ($R_{O/F}$) and in (b) air-dried samples relative to freeze-dried samples ($R_{A/F}$). Errors
 650 for each ratio were calculated by propagating errors for filter-normalized peak
 651 abundances (~10%). The two clusters of data points at chain lengths 15 and 17 represent
 652 isomers of the same size molecule. The pair of 15 chain length compounds corresponds
 653 to the iso- and anteiso-methyl-branched fatty acids from left to right, respectively. The
 654 leftmost data point of the 17 chain length pair corresponds to the iso-methyl-branched
 655 fatty acid, while the rightmost data point corresponds to the heterocyclic isomer cis-9,10-
 656 methylenehexadecanoate. (c) $R_{O/F}$ and $R_{A/F}$ plotted on the same axes alongside ratios of
 657 oven-dried (triangle) or air-dried (star) blank compound abundances to freeze-dried blank
 658 compound abundances. The relative errors of these ratios in the deployment blanks are
 659 <1% and are thus not shown. (d) Absolute normalized and blank-corrected peak areas in
 660 the freeze-dried samples.



661

662 Figure 6. (a-b) Ratios of filter-normalized and blank-corrected peak areas of seven
 663 alcohols/sterols in (a) oven-dried particle samples relative to freeze-dried samples ($R_{O/F}$)
 664 and in (b) air-dried samples relative to freeze-dried samples ($R_{A/F}$). Errors for each ratio
 665 were calculated by propagating errors for filter-normalized peak abundances (~10%). The
 666 x-axis is molar weight, which matches the compounds listed in Table 3. (c) Absolute
 667 normalized blank-corrected peak areas of alcohols/sterols in the freeze-dried sample.
 668 Quantities in panels d-f are analogous to quantities in a-c, but are not blank-corrected.
 669 Relative errors for ratios in d-e, not plotted, are <1%.

670

671

672 **Acknowledgements**

673

674 Ulrich Loic Kakou and Paul Lerner participated in the field collection of samples;

675 Al Gagnon, Mary Lardie, Jordon Hemingway, Kyrstin Fornace and Guillaume Soulet

676 helped with the bulk, isotope and RPO analyses. Horst Marschall assisted in use of the

677 scanning electron microscope. Elizabeth Canuel provided insightful comments and

678 advice in experimental design of this study. This research was funded by the National

679 Science Foundation (NSF) Graduate Research Fellowship program and the NSF

680 Cooperative Agreement for the Operation of a National Ocean Sciences Accelerator

681 Mass Spectrometry Facility (OCE-0753487).

682

683

Table S1. Abundances of select fatty acids, alcohols and sterols quantified in freeze-dried, air-dried and oven-dried particle samples (POC1+2+3) and deployment blanks (db1+2). The abundances are represented as peak areas normalized to the total active area of a QMA filter, 125 cm², but are not blank-corrected. “Fraction from blank” is the abundance of each compound in the freeze-dried, oven-dried or air-dried sample deployment blank filters relative to the abundance observed in the freeze-dried, oven-dried or air-dried particle sample filters, respectively. The R_{O/F} and R_{A/F} values are ratios of either oven-dried or air-dried compound peak areas to freeze-dried compound peak areas in the blank filters or in the particle samples prior to blank subtraction. Note that these ratios differ in samples and blanks, which justifies the choice to subtract blank contributions from sample peak abundances before calculating the ratios presented in Section 3.3. The straight-chain fatty acids are named as C followed by chain length: number of double bonds. The branched fatty acids are named with a “C” followed by just the chain length.

Sample or blank	Treatment	Compound	Normalized Peak Area	Fraction from blank	R _{O/F} or R _{A/F}
--	--	--		%	--
POC1+2+3	Freeze	C12:0	230,730,000	3%	
POC1+2+3	Freeze	C13:0	23,175,000	10%	
POC1+2+3	Freeze	C14:1	15,356,000	10%	
POC1+2+3	Freeze	C14:0	4,934,400,000	1%	
POC1+2+3	Freeze	C15, branched ^a	172,350,000	2%	
POC1+2+3	Freeze	C15, branched ^b	104,040,000	4%	
POC1+2+3	Freeze	C15:0	265,890,000	10%	
POC1+2+3	Freeze	C16, branched	151,780,000	2%	
POC1+2+3	Freeze	C16:1	3,254,100,000	0.2%	
POC1+2+3	Freeze	C16:0	16,057,000,000	11%	
POC1+2+3	Freeze	C17, branched ^a	38,213,000	22%	
POC1+2+3	Freeze	C17:1	87,019,000	14%	

POC1+2+3	Freeze	C17, branched ^c	46,106,000	16%	
POC1+2+3	Freeze	C17:0	222,260,000	20%	
POC1+2+3	Freeze	C18:3	674,290,000	0%	
POC1+2+3	Freeze	C18:2 ^d	1,729,500,000	0.5%	
POC1+2+3	Freeze	C18:2 ^e	2,137,900,000	1%	
POC1+2+3	Freeze	C18:1 ^f	2,524,800,000	0%	
POC1+2+3	Freeze	C18:1 ^g	829,260,000	1%	
POC1+2+3	Freeze	C18:0	5,869,600,000	28%	
POC1+2+3	Freeze	C20:4	1,408,700,000	0%	
POC1+2+3	Freeze	C20:3	135,710,000	0%	
POC1+2+3	Freeze	C20:2	49,256,000	7%	
POC1+2+3	Freeze	C20:1	81,094,000	2%	
POC1+2+3	Freeze	C20:0	91,031,000	13%	
POC1+2+3	Freeze	C22:1	22,969,000	23%	
POC1+2+3	Freeze	C22:0	52,069,000	3%	
POC1+2+3	Freeze	C24:0	49,969,000	4%	
POC1+2+3	Freeze	1-hexadecanol	10,306,000	51%	
POC1+2+3	Freeze	Phytol	385,380,000	0.4%	
POC1+2+3	Freeze	Cholesterol	104,050,000	1%	
POC1+2+3	Freeze	5 α -cholestan-3- β -ol	22,578,000	0%	
POC1+2+3	Freeze	Brassicasterol	100,870,000	0%	
POC1+2+3	Freeze	Stigmasterol	33,172,000	0%	
POC1+2+3	Freeze	Gorgosterol	42,698,000	0%	
POC1+2+3	Oven	C12:0	45,326,000	58%	0.20
POC1+2+3	Oven	C13:0	11,176,000	29%	0.48
POC1+2+3	Oven	C14:1	4,112,900	0%	0.27
POC1+2+3	Oven	C14:0	1,824,200,000	5%	0.37
POC1+2+3	Oven	C15, branched ^a	73,059,000	5%	0.42
POC1+2+3	Oven	C15, branched ^b	51,341,000	15%	0.49
POC1+2+3	Oven	C15:0	128,160,000	31%	0.48
POC1+2+3	Oven	C16, branched	34,648,000	14%	0.23
POC1+2+3	Oven	C16:1	1,393,700,000	0.3%	0.43
POC1+2+3	Oven	C16:0	7,295,100,000	25%	0.45
POC1+2+3	Oven	C17, branched ^a	22,645,000	51%	0.59
POC1+2+3	Oven	C17:1	49,980,000	34%	0.57
POC1+2+3	Oven	C17, branched ^c	26,804,000	27%	0.58
POC1+2+3	Oven	C17:0	103,250,000	47%	0.46
POC1+2+3	Oven	C18:3	83,036,000	0%	0.12
POC1+2+3	Oven	C18:2 ^d	458,330,000	2%	0.27
POC1+2+3	Oven	C18:2 ^e	419,150,000	3%	0.20
POC1+2+3	Oven	C18:1 ^f	1,084,600,000	0%	0.43
POC1+2+3	Oven	C18:1 ^g	366,900,000	1%	0.44
POC1+2+3	Oven	C18:0	2,045,600,000	67%	0.35

POC1+2+3	Oven	C20:4	168,990,000	0%	0.12
POC1+2+3	Oven	C20:3	27,352,000	9%	0.20
POC1+2+3	Oven	C20:2	21,258,000	7%	0.43
POC1+2+3	Oven	C20:1	33,895,000	7%	0.42
POC1+2+3	Oven	C20:0	52,092,000	18%	0.57
POC1+2+3	Oven	C22:1	9,888,500	62%	0.43
POC1+2+3	Oven	C22:0	35,163,000	9%	0.68
POC1+2+3	Oven	C24:0	36,053,000	7%	0.72
POC1+2+3	Oven	1-hexadecanol	10,266,000	36%	1.00
POC1+2+3	Oven	Phytol	353,840,000	0.4%	0.92
POC1+2+3	Oven	Cholesterol	100,910,000	0%	0.97
POC1+2+3	Oven	5 α -cholestan-3- β -ol	24,272,000	0%	1.08
POC1+2+3	Oven	Brassicasterol	89,803,000	0%	0.89
POC1+2+3	Oven	Stigmasterol	34,373,000	0%	1.04
POC1+2+3	Oven	Gorgosterol	24,195,000	0%	0.57
POC1+2+3	Air	C12:0	53,204,000	40%	0.23
POC1+2+3	Air	C13:0	8,572,600	28%	0.37
POC1+2+3	Air	C14:1	5,493,400	0%	0.36
POC1+2+3	Air	C14:0	2,421,700,000	7%	0.49
POC1+2+3	Air	C15, branched ^a	97,270,000	4%	0.56
POC1+2+3	Air	C15, branched ^b	62,692,000	9%	0.60
POC1+2+3	Air	C15:0	173,380,000	26%	0.65
POC1+2+3	Air	C16, branched	65,582,000	9%	0.43
POC1+2+3	Air	C16:1	1,485,300,000	0.3%	0.46
POC1+2+3	Air	C16:0	11,687,000,000	31%	0.73
POC1+2+3	Air	C17, branched ^a	41,455,000	45%	1.08
POC1+2+3	Air	C17:1	73,241,000	35%	0.84
POC1+2+3	Air	C17, branched ^c	36,104,000	19%	0.78
POC1+2+3	Air	C17:0	189,910,000	50%	0.85
POC1+2+3	Air	C18:3	124,130,000	0%	0.18
POC1+2+3	Air	C18:2 ^d	713,190,000	2%	0.41
POC1+2+3	Air	C18:2 ^e	564,150,000	0%	0.26
POC1+2+3	Air	C18:1 ^f	1,280,800,000	2%	0.51
POC1+2+3	Air	C18:1 ^g	433,400,000	2%	0.52
POC1+2+3	Air	C18:0	5,243,000,000	68%	0.89
POC1+2+3	Air	C20:4	249,840,000	0%	0.18
POC1+2+3	Air	C20:3	51,672,000	0%	0.38
POC1+2+3	Air	C20:2	24,210,000	3%	0.49
POC1+2+3	Air	C20:1	34,600,000	4%	0.43
POC1+2+3	Air	C20:0	79,482,000	35%	0.87
POC1+2+3	Air	C22:1	17,952,000	56%	0.78
POC1+2+3	Air	C22:0	41,130,000	9%	0.79
POC1+2+3	Air	C24:0	52,335,000	7%	1.05

POC1+2+3	Air	1-hexadecanol	8,954,100	51%	0.87
POC1+2+3	Air	Phytol	321,560,000	1%	0.83
POC1+2+3	Air	Cholesterol	91,996,000	0%	0.88
POC1+2+3	Air	5 α -cholestan-3- β -ol	21,919,000	0%	0.97
POC1+2+3	Air	Brassicasterol	88,627,000	0%	0.88
POC1+2+3	Air	Stigmasterol	29,892,000	0%	0.90
POC1+2+3	Air	Gorgosterol	29,202,000	0%	0.68
db1+2	Freeze	C12:0	6,916,400		
db1+2	Freeze	C13:0	2,308,700		
db1+2	Freeze	C14:1	1,517,400		
db1+2	Freeze	C14:0	73,738,000		
db1+2	Freeze	C15, branched ^a	2,668,500		
db1+2	Freeze	C15, brancheddb1+2	4,570,200		
db1+2	Freeze	C15:0	25,625,000		
db1+2	Freeze	C16, branched	3,793,500		
db1+2	Freeze	C16:1	6,860,900		
db1+2	Freeze	C16:0	1,831,900,000		
db1+2	Freeze	C17, branched ^a	8,362,700		
db1+2	Freeze	C17:1	12,346,000		
db1+2	Freeze	C17, branched ^c	7,156,200		
db1+2	Freeze	C17:0	43,444,000		
db1+2	Freeze	C18:3	-		
db1+2	Freeze	C18:2 ^d	8,610,200		
db1+2	Freeze	C18:2 ^e	25,589,000		
db1+2	Freeze	C18:1 ^f	-		
db1+2	Freeze	C18:1 ^g	8,262,500		
db1+2	Freeze	C18:0	1,620,100,000		
db1+2	Freeze	C20:4	-		
db1+2	Freeze	C20:3	-		
db1+2	Freeze	C20:2	3,576,000		
db1+2	Freeze	C20:1	1,876,600		
db1+2	Freeze	C20:0	11,724,000		
db1+2	Freeze	C22:1	5,301,600		
db1+2	Freeze	C22:0	1,777,600		
db1+2	Freeze	C24:0	1,956,900		
db1+2	Freeze	1-hexadecanol	5,209,300		
db1+2	Freeze	Phytol	1,421,900		
db1+2	Freeze	Cholesterol	1,341,700		
db1+2	Freeze	5 α -cholestan-3- β -ol	-		
db1+2	Freeze	Brassicasterol	-		
db1+2	Freeze	Stigmasterol	-		
db1+2	Freeze	Gorgosterol	-		
db1+2	Oven	C12:0	26,156,000		3.78

db1+2	Oven	C13:0	3,271,000	1.42
db1+2	Oven	C14:1	-	0.00
db1+2	Oven	C14:0	97,448,000	1.32
db1+2	Oven	C15, branched ^a	3,881,200	1.45
db1+2	Oven	C15, branched ^b	7,740,500	1.69
db1+2	Oven	C15:0	39,432,000	1.54
db1+2	Oven	C16, branched	4,827,200	1.27
db1+2	Oven	C16:1	4,476,400	0.65
db1+2	Oven	C16:0	1,842,100,000	1.01
db1+2	Oven	C17, branched ^a	11,587,000	1.39
db1+2	Oven	C17:1	16,773,000	1.36
db1+2	Oven	C17, branched ^c	7,352,200	1.03
db1+2	Oven	C17:0	48,682,000	1.12
db1+2	Oven	C18:3	-	-
db1+2	Oven	C18:2 ^d	7,065,000	0.82
db1+2	Oven	C18:2 ^e	10,735,000	0.42
db1+2	Oven	C18:1 ^f	-	-
db1+2	Oven	C18:1 ^g	5,008,500	0.61
db1+2	Oven	C18:0	1,375,200,000	0.85
db1+2	Oven	C20:4	-	-
db1+2	Oven	C20:3	2,349,100	-
db1+2	Oven	C20:2	1,594,100	0.45
db1+2	Oven	C20:1	2,336,500	1.25
db1+2	Oven	C20:0	9,324,700	0.80
db1+2	Oven	C22:1	6,095,700	1.15
db1+2	Oven	C22:0	3,015,400	1.70
db1+2	Oven	C24:0	2,658,700	1.36
db1+2	Oven	1-hexadecanol	3,667,600	0.70
db1+2	Oven	Phytol	1,306,600	0.92
db1+2	Oven	Cholesterol	-	0.00
db1+2	Oven	5 α -cholestan-3- β -ol	-	-
db1+2	Oven	Brassicasterol	-	-
db1+2	Oven	Stigmasterol	-	-
db1+2	Oven	Gorgosterol	-	-
db1+2	Air	C12:0	21,406,000	3.09
db1+2	Air	C13:0	2,365,800	1.02
db1+2	Air	C14:1	-	0.00
db1+2	Air	C14:0	162,790,000	2.21
db1+2	Air	C15, branched ^a	3,802,800	1.43
db1+2	Air	C15, branched ^{b1+2}	5,369,700	1.17
db1+2	Air	C15:0	44,762,000	1.75
db1+2	Air	C16, branched	5,673,800	1.50
db1+2	Air	C16:1	4,857,200	0.71

db1+2	Air	C16:0	3,633,300,000	1.98
db1+2	Air	C17, branched ^a	18,454,000	2.21
db1+2	Air	C17:1	25,480,000	2.06
db1+2	Air	C17, branched ^c	6,793,300	0.95
db1+2	Air	C17:0	94,158,000	2.17
db1+2	Air	C18:3	-	-
db1+2	Air	C18:2 ^d	13,530,000	1.57
db1+2	Air	C18:2 ^e	-	0.00
db1+2	Air	C18:1 ^f	22,137,000	-
db1+2	Air	C18:1 ^g	9,540,200	1.15
db1+2	Air	C18:0	3,576,200,000	2.21
db1+2	Air	C20:4	-	-
db1+2	Air	C20:3	-	-
db1+2	Air	C20:2	701,330	0.20
db1+2	Air	C20:1	1,291,300	0.69
db1+2	Air	C20:0	28,169,000	2.40
db1+2	Air	C22:1	10,085,000	1.90
db1+2	Air	C22:0	3,865,200	2.17
db1+2	Air	C24:0	3,677,500	1.88
db1+2	Air	1-hexadecanol	4,578,900	0.88
db1+2	Air	Phytol	4,389,300	3.09
db1+2	Air	Cholesterol	-	-
db1+2	Air	5 α -cholestan-3- β -ol	-	-
db1+2	Air	Brassicasterol	-	-
db1+2	Air	Stigmasterol	-	-
db1+2	Air	Gorgosterol	-	-

^aiso

^banteiso

^ccis-9,10-methylenehexadecanoate

^dcis-9,12-octadecadienoate

^etrans-9,12-octadecadienoate

^fcis-9-octadecenoate

^gtrans-9-octadecenoate